

Contrasting Momentum-Selective Spin-Density-Wave Gaps in Bilayer and Trilayer Nickelates

Jun Shu^{1,2,10}, Jun Shen¹✉, Xiaoxiang Zhou^{3,10}, Yinghao Zhu⁷, Qingsong Wang¹, Dengjing Wang², Weihong He³ Jie Yuan^{4,5}, Kui Jin^{4,5,6}, Dawei Shen³ Congcong Le³, Jun Zhao⁷✉, Zengyi Du³✉, Ge He¹✉, Donglai Feng³✉

¹ School of Mechanical Engineering, Beijing Institute of Technology, Beijing 100081, China

² Department of Applied Physics, Wuhan University of Science and Technology, Wuhan 430081, China

³ Hefei National Laboratory, and New Cornerstone Science Laboratory, Hefei, Anhui 230088, China

⁴ Beijing National Laboratory for Condensed Matter Physics, Institute of Physics, Chinese Academy of Sciences, Beijing 100190, China

⁵ School of Physical Sciences, University of Chinese Academy of Sciences, Beijing 100049, China

⁶ Songshan Lake Materials Laboratory, Dongguan, Guangdong 523808, China

⁷ State Key Laboratory of Surface Physics and Department of Physics, Fudan University, Shanghai 200433, China

¹⁰ These authors contributed equally: Jun Shu and Xiaoxiang Zhou

✉ e-mail: jshen@bit.edu.cn; zhaoj@fudan.edu.cn duzengyi@hfnl.cn; ge.he@bit.edu.cn; dlfeng@hfnl.cn

ABSTRACT

Resolving where the density-wave gap opens in momentum space is essential for identifying the microscopic origin of the instability in layered nickelates. Using polarization-resolved electronic Raman scattering, we map the momentum selectivity of the spin-density-wave (SDW) gap in trilayer $\text{La}_4\text{Ni}_3\text{O}_{10}$. We observe a SDW-induced redistribution of spectral weight on both the α pocket at the Brillouin-zone centre and a portion of the β pocket near the zone boundary, characterized by gap energies of approximately 55 meV. In contrast, no comparable spectral weight suppression is observed along the diagonal region of β pockets, implying little or no gap opening. This gap topology contrasts sharply with that in $\text{La}_3\text{Ni}_2\text{O}_7$, where anisotropic SDW gaps open solely on the β pocket. Our results establish a distinct momentum-space gap topology between bilayer and trilayer nickelates, placing new constraints on the ordering wave vector and the mechanism of the density-wave instability relevant to superconductivity.

INTRODUCTION

Layered nickelate superconductors, including $\text{La}_4\text{Ni}_3\text{O}_{10}$ and $\text{La}_3\text{Ni}_2\text{O}_7$, exhibit markedly different superconducting transition temperatures despite closely related crystal structures and electronic band topologies [1–7]. Both compounds host a density-wave (DW) instability in the normal state at $T_{\text{DW}} \approx 140\text{--}150$ K [3, 8–29], widely discussed in terms of spin- and/or charge-density-wave (SDW/CDW) formation. This ordering substantially reshapes the low-energy electronic structure, making the momentum dependence of the associated gap a key ingredient for understanding how superconductivity emerges.

Rather than providing a unified picture, existing experiments probe complementary but incomplete aspects of the DW state in $\text{La}_4\text{Ni}_3\text{O}_{10}$. X-ray scattering and optical measurements [20, 21] unambiguously establish the presence of DW order and a finite gap scale, respectively, but lack the combined energy and momentum resolution required to determine where the gap opens in reciprocal space. Momentum-resolved probes, such as angle-resolved photoemission spectroscopy (ARPES) and electronic Raman scattering [22–25, 30], access this information more directly but have so far yielded mutually inconsistent conclusions regarding the involved Fermi-surface pockets. Real-space imaging by scanning tunneling mi-

croscopy (STM) further reveals a DW modulation and constrains the ordering wave vector, but does not directly resolve the momentum-dependent gap structure [26]. As a result, the topology of the DW gap in momentum space remains unresolved.

Symmetry-resolved electronic Raman scattering is a powerful probe of momentum-dependent gap formation and has been successfully applied to reveal both DW gaps and superconducting gap openings in cuprates and iron-based superconductors [31, 32]. Our previous polarization-resolved electronic Raman scattering study on $\text{La}_3\text{Ni}_2\text{O}_7$ demonstrated that the SDW gap opens in a highly momentum-selective manner [19]. In that system, an anisotropic SDW gap with strong-coupling character develops on the β pocket, while the α pocket remains ungapped. This momentum-selective SDW gap structure provided a consistent framework for reconciling the seemingly disparate results reported by ARPES [14, 15, 33, 34], optical conductivity [17, 18].

In this work, we use polarization- and symmetry-resolved electronic Raman scattering to directly determine the momentum-selective structure of the SDW gap in $\text{La}_4\text{Ni}_3\text{O}_{10}$. By comparing with the SDW gap topology previously established in $\text{La}_3\text{Ni}_2\text{O}_7$ [19], we uncover qualitative differences in both the momentum dependence and coherence of the SDW state. In $\text{La}_4\text{Ni}_3\text{O}_{10}$, Raman spectra reveal a pronounced SDW-induced spec-

tral weight redistribution near the Brillouin-zone (BZ) center (α pocket) and boundary (β pockets), corresponding to a characteristic gap scale of ~ 55 meV, while no comparable suppression is observed along the Γ -M direction of the β pockets, contrasting sharply with $\text{La}_3\text{Ni}_2\text{O}_7$, where strong-coupling SDW gaps open on the β pocket. These observations indicate that the incommensurate SDW wave vector in $\text{La}_4\text{Ni}_3\text{O}_{10}$ predominantly connects the α and β pockets near the X/Y points (Q_2 in Fig. 1b), rather than the α - β nesting along the Γ -M direction (Q_1). Our results establish a distinct momentum-space SDW gap topology in $\text{La}_4\text{Ni}_3\text{O}_{10}$, providing new constraints on the microscopic origin of density-wave order in layered nickelates.

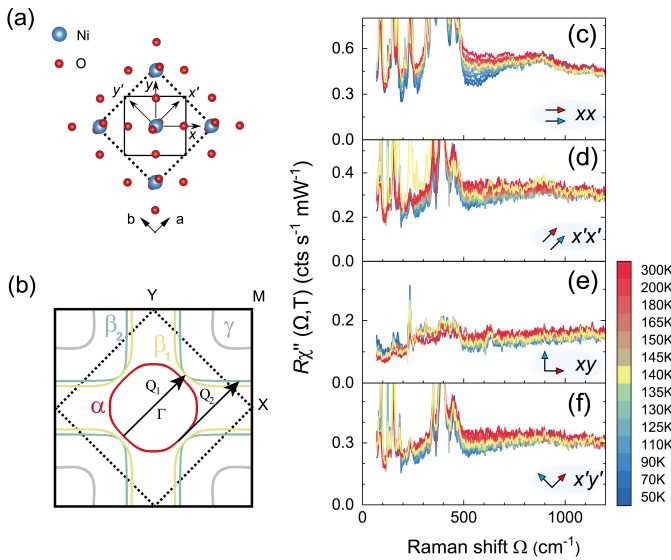


Figure 1. Definition of the Ni–O unit cell, photon polarizations, Fermi pockets, and Raman responses in different polarization configurations. (a) Solid (dashed) lines indicate the 1-Ni (2-Ni) unit cell. The x and y axes are aligned along the Ni–O–Ni bond directions, while the x' and y' polarizations are rotated by 45° clockwise, corresponding to the Ni–Ni directions. (b) Schematic Fermi surface obtained from a tight-binding model with α (red), β_1 (yellow), β_2 (green), and γ (grey) pockets (see Supplementary Materials F for details). Black arrows denote candidate scattering wave vectors: \mathbf{Q}_1 and \mathbf{Q}_2 . (c–f) Temperature dependence of the electronic continuum measured in the xx , $x'x'$, xy , and $x'y'$ channels.

RESULTS

$\text{La}_4\text{Ni}_3\text{O}_{10}$ single crystals were synthesized using a vertical optical-image floating-zone furnace with appropriate oxygen pressure [2] (see Supplementary Materials A for details), exhibiting a characteristic DW transition near 140 K. Raman scattering measurements were performed using a commercial Raman spectrometer in confocal ge-

ometry (see Supplementary Materials B for details). Four polarization configurations were employed: $\hat{x}\hat{x}$, $\hat{x}\hat{y}$, $\hat{x}'\hat{x}'$, and $\hat{x}'\hat{y}'$, where \hat{x} is oriented along the Ni–O–Ni bond and \hat{x}' along the Ni–Ni direction [Fig. 1(a)].

$\text{La}_4\text{Ni}_3\text{O}_{10}$ belongs to the C_{2h} point group at ambient pressure, which hosts a number of Raman-active phonon modes according to factor group analysis (details can be found in the Supplemental Materials C and Refs. [24, 25, 30, 35]). All phonon modes appear below 500 cm^{-1} in our Raman spectra. The phonon results are discussed in the Supplemental Materials D, while here we focus on the electronic Raman response.

Figure 1(c–f) shows the electronic continuum in all four polarization configurations. The continuum exhibits a clear spectral weight loss below 1000 cm^{-1} in the $\hat{x}\hat{x}$, $\hat{x}'\hat{x}'$, and $\hat{x}'\hat{y}'$ channels as the temperature decreases from ≈ 140 K. The intensity is reduced by up to 50% in the $\hat{x}\hat{x}$ channel and by approximately 30% in the $\hat{x}'\hat{x}'$ and $\hat{x}'\hat{y}'$ channels at 500 cm^{-1} . In contrast, the spectral weight remains nearly unchanged in the $\hat{x}\hat{y}$ channel. These results are consistent with previous studies [24, 25], demonstrating reproducibility across different sample sources.

Although $\text{La}_4\text{Ni}_3\text{O}_{10}$ has a monoclinic structure, if we focus solely on the Ni–O plane, as we have done previously in $\text{La}_3\text{Ni}_2\text{O}_7$ [19] the electronic Raman response can be analyzed using a pseudo- D_{4h} symmetry, similar to approaches in cuprates [31] and Fe-based superconductors [32]. This framework allows the spectra to be decomposed into three orthogonal symmetries: A_{1g} , B_{1g} , and B_{2g} . The method for isolating spectra in pure symmetries is described in the Supplemental Materials E. Using this decomposition, we can resolve excitations in different regions of the BZ based on symmetry-imposed selection rules. Following the analogy with tetragonal materials, within the BZ defined for a 1-Ni unit cell, the A_{1g} channel primarily probes electronic excitations near the BZ center (Γ point) and corner (M point). In contrast, the B_{1g} channel predominantly selects excitations near the BZ boundary around X and Y points, while the B_{2g} channel is most sensitive to excitations along the diagonal directions of the BZ [see the insets in the top-right corner of Fig. 2(a–c) and Supplementary Materials E].

Figure 2 presents the Raman spectra in the A_{1g} , B_{1g} , and B_{2g} symmetries. In the A_{1g} channel, a peak near 900 cm^{-1} is clearly visible at both 50 K and 140 K, with no discernible energy shift. This feature persists even at 300 K. Suthar *et al.* have attributed this peak to the opening of an SDW gap [25], although our data suggest a different interpretation (may be a multi-phonon mode or even side effect from the surface). Specifically, we observe instead only a dip feature below 800 cm^{-1} in the difference spectra [$\chi''(50\text{ K}) - \chi''(140\text{ K})$] of the A_{1g} channel (see Fig. 2(a)). In the B_{1g} channel, the difference spectra exhibit a dip–hump structure with a crossing point near 800 cm^{-1} , consistent with a gap-opening feature, albeit significantly broadened (see Fig. 2(b)). By contrast,

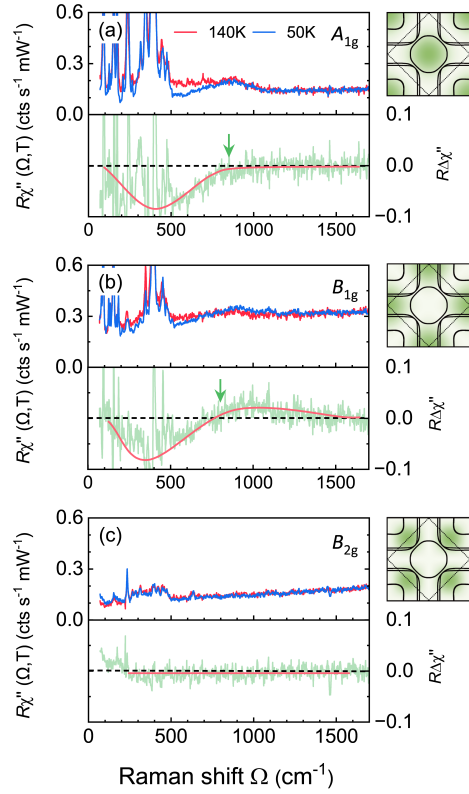


Figure 2. Electronic continuum spectra in pure symmetries at 50 K and 140 K. Difference spectra $[\chi''(50 \text{ K}) - \chi''(140 \text{ K})]$ are shown as green curves. Red lines serve as guides to the eye. Insets: Crystal harmonics, proportional to the Raman vertices in the first Brillouin zone, superimposed on the Fermi pockets for the A_{1g} , B_{1g} , and B_{2g} symmetries.

no discernible spectral changes are observed in the B_{2g} channel across T_{SDW} (see Fig. 2(c)).

Table I. Comparison of SDW features between $\text{La}_4\text{Ni}_3\text{O}_{10}$ and $\text{La}_3\text{Ni}_2\text{O}_7$.

	$T_{\text{SDW}}(\text{K})$	Q_{SDW}		$\Delta_{\text{SDW}}(\text{meV})$
		Q vector	BZ	
$\text{La}_4\text{Ni}_3\text{O}_{10}$	~ 140	(0.31,0.31,0)	1-Ni	$\Delta_{A_{1g}} \sim 56$
		(0.0,0.61,0) [20]	2-Ni	$\Delta_{B_{1g}} \sim 55$
$\text{La}_3\text{Ni}_2\text{O}_7$	~ 150	(0.25,0.25,0) [8]	1-Ni	$\Delta_{B_{1g}} \sim 37$
		(0,0.5,0)	2-Ni	$\Delta_{B_{2g}} \sim 23$

DISCUSSION

The nature of the DW order in $\text{La}_4\text{Ni}_3\text{O}_{10}$ has been widely studied [20–23, 35–37], with the debate centering on two key issues. The first concerns the driving mechanism of the instability, namely whether it originates from spin, charge, or coupled spin–charge degrees of freedom.

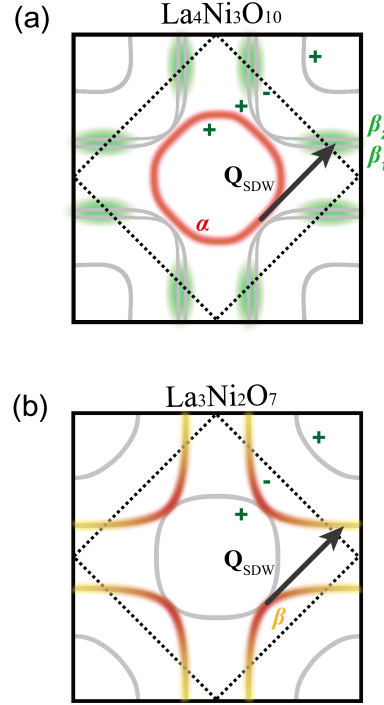


Figure 3. Comparison of density-wave gaps and candidate scattering vectors in $\text{La}_4\text{Ni}_3\text{O}_{10}$ and $\text{La}_3\text{Ni}_2\text{O}_7$. Gapped Fermi pockets are highlighted in (a) α pocket and β pocket near XY points of $\text{La}_4\text{Ni}_3\text{O}_{10}$ and (b) β pocket of $\text{La}_3\text{Ni}_2\text{O}_7$. Black arrows indicate possible scattering wave vectors. '+' and '-' signs denote the parity of the bands determined by the layer index (top and bottom Ni-O planes). The colored shading superimposed on the Fermi surface pockets highlights the momentum regions in which energy gaps open.

The second concerns the detailed nature of the gap opening and the associated ordering wave vector. Regarding the driving mechanism, our temperature-dependent Raman measurements do not reveal detectable zone-folded phonons across T_{DW} (see Supplementary Materials D), and no sharp collective amplitude mode has been reported so far. Compared with canonical lattice-driven CDW systems, such as transition-metal dichalcogenides [38, 39], kagome metals [40], and rare-earth tritellurides (ReTe_3) [41], where multiple zone-folded modes and a pronounced amplitude mode are readily resolved in Raman spectra, this lack of clear lattice signatures disfavors a strongly lattice-driven CDW scenario in $\text{La}_4\text{Ni}_3\text{O}_{10}$. Instead, our results disfavor a strongly lattice-driven CDW scenario and are consistent with a primarily electronic DW state with a dominant spin component. This conclusion is in line with our previous $\text{La}_3\text{Ni}_2\text{O}_7$ Raman study [19] and with STM observations that visualize a CDW modulation likely intertwined with (and possibly secondary to) the underlying SDW or

der [26]. Following the STM work, a question remains as to whether the SDW ordering wave vector is determined by nesting between the α and β pockets or by nesting between parallel segments of the β pocket along the (π, π) direction. In this work, our results provide evidence that favors the α - β nesting scenario, as discussed in detail below.

According to the Raman selection rules, the A_{1g} spectral-weight loss points to a possible gap opening on either the α or γ pocket, or both. DFT calculations suggest that a nearly dispersionless flat band on the γ pocket dominated by Ni d_{z^2} character is present [27, 28], thus, making a gap opening on the α pocket a more plausible scenario. The dip-hump feature observed in the B_{1g} channel suggests a gap opening on the β pockets near the X and Y points (β_1 or β_2 or both, normally, Raman experiments cannot distinguish them), which has not been reported previously. In contrast, the absence of significant changes in the B_{2g} channel indicates that the electrons occupying the β pockets near the diagonal region of the BZ likely play only a minor role in the SDW formation. Note that Suthar *et al.* argued that the absence of the gap opening feature in B_{2g} symmetry is due to the negligible next-nearest-neighbor hopping, resulting in a nearly zero Raman form factor [25]. In contrast, a pronounced gap feature is clearly observed in the B_{2g} channel of $\text{La}_3\text{Ni}_2\text{O}_7$ [19]. Given the fact both of the compounds share quite similar band structure, this comparison suggests that the absence of a gap opening in the B_{2g} channel in $\text{La}_4\text{Ni}_3\text{O}_{10}$ is likely due to intrinsic electronic structure properties, where no gap opens in the corresponding region.

These results enable a direct comparison of the SDW properties in $\text{La}_4\text{Ni}_3\text{O}_{10}$ and $\text{La}_3\text{Ni}_2\text{O}_7$ (see Tab. I and Fig. 3). In $\text{La}_3\text{Ni}_2\text{O}_7$, anisotropic gaps open on the β pocket with a pronounced coherence peaks [19]. By contrast, in $\text{La}_4\text{Ni}_3\text{O}_{10}$, gaps open on the α and β pockets near X/Y points (β_1 or β_2 or both), but the coherence effect is extremely weak and barely discernible. Specifically, in our previous work, we discussed the possibility that a screening effect in the A_{1g} channel could have resulted in the failure to observe a gap on the α pocket in $\text{La}_3\text{Ni}_2\text{O}_7$ [19]. With a direct comparison between $\text{La}_3\text{Ni}_2\text{O}_7$ and $\text{La}_4\text{Ni}_3\text{O}_{10}$ now available, we have examined the effect of Coulomb screening in both systems using a tight-binding model (see Supplementary Materials G for details). We found that the screening effect reduces the gap excitation intensity by 40% and 50% for $\text{La}_4\text{Ni}_3\text{O}_{10}$ and $\text{La}_3\text{Ni}_2\text{O}_7$, respectively. These comparable reductions indicate that screening alone is insufficient to account for the complete absence of a gap-related excitation in the A_{1g} symmetry of $\text{La}_3\text{Ni}_2\text{O}_7$. We therefore infer that α pocket in $\text{La}_3\text{Ni}_2\text{O}_7$ is unlikely to host an SDW gap.

Based on the observed gap-opening characteristics, we propose possible scattering vectors connecting the Fermi

pockets. X-ray, neutron scattering, and STM experiments have suggested a characteristic wave vector \mathbf{Q}_1 (see Fig. 1) that connects the α and β pockets [20, 42]. Such a scenario would induce a gap on both the α and β pockets. In particular, restricted by the mirror symmetry between the top and bottom Ni-O planes in both $\text{La}_3\text{Ni}_2\text{O}_7$ and $\text{La}_4\text{Ni}_3\text{O}_{10}$, and considering the interplane antiferromagnetic coupling, the nesting vector would connect bands of opposite parity (marked with '+' and '-' signs in Fig. 3) [43, 44]. However, two aspects of this picture conflict with our Raman results. First, there is no gap opening on the α pocket in $\text{La}_3\text{Ni}_2\text{O}_7$ [19]. Second, we fail to observe a gap opening in the diagonal region of the BZ on the β pockets in $\text{La}_4\text{Ni}_3\text{O}_{10}$, even though this region satisfies the nesting condition perfectly between the α and β pockets. To understand our results, we propose a scattering vector \mathbf{Q}_{SDW} that connects the α pocket and β pocket (near the X/Y points) in $\text{La}_4\text{Ni}_3\text{O}_{10}$ and the β pocket itself [between $(\pi/2, -\pi/2)$ and $(\pi, 0)$] in $\text{La}_3\text{Ni}_2\text{O}_7$ (Fig. 3). This configuration naturally accounts for the observed gap openings in both systems. However, it conflicts with the mainstream nesting picture (\mathbf{Q}_1 in Fig. 1b) discussed above. To reconcile this discrepancy, one would need to consider momentum-dependent scattering and/or strong-coupling mechanism [14, 17, 33], which requires further investigation.

In summary, we have employed polarization-resolved Raman scattering to investigate the density-wave state in $\text{La}_4\text{Ni}_3\text{O}_{10}$. By decomposing the spectra into distinct symmetries, we identified spectral-weight anomalies that signal momentum-selective gap openings on the α and β pockets. This observation is inconsistent with the commonly proposed scattering vector \mathbf{Q}_1 , and instead supports an alternative vector \mathbf{Q}_2 connecting the α and β pockets near the X/Y points. A comparison with $\text{La}_3\text{Ni}_2\text{O}_7$ further reveals the distinctive momentum selectivity of the SDW order in $\text{La}_3\text{Ni}_2\text{O}_7$ and $\text{La}_4\text{Ni}_3\text{O}_{10}$, and provides key insights into its connection with superconductivity in layered nickelates.

Note added. During the preparation of our manuscript, we became aware of a recent ARPES study on $\text{La}_4\text{Ni}_3\text{O}_{10}$ posted on arXiv [45], reporting momentum-selective gap opening. These observations are nearly consistent with our results.

We thank George Sawatzky, Jiangping Hu, Tao Xiang, Xianin Wu, Ruizhen Huang and Wei Li for fruitful discussions. This work is supported by the National Key Basic Research Program of China (Grants Nos. 2024YFF0727103), the National Natural Science Foundation of China (Grants Nos. 12474473, U23A6015, 12104490, 12375331), D.L.F acknowledges the support by the New Cornerstone Science Foundation (Grant No. NCI202211), and the Innovation Program for Quantum Science and Technology (Grant No. 2021ZD0302803). J.Y. and K.J. acknowledge the support by the CAS Project for Young Scientists in Ba-

sic Research (Grant No. 2022YSBR-048). The work at Fudan University was supported by the Key Program of the National Natural Science Foundation of China (12234006), the Innovation Program for Quantum Science and Technology (2024ZD0300100), the National Key R&D Program of China (2022YFA1403202), and the Shanghai Municipal Science and Technology Major Project (2019SHZDZX01).

[1] H. Sun, M. Huo, X. Hu, J. Li, Z. Liu, Y. Han, L. Tang, Z. Mao, P. Yang, B. Wang, J. Cheng, D.-X. Yao, G.-M. Zhang, and M. Wang, Signatures of superconductivity near 80 K in a nickelate under high pressure, *Nature* **621**, 493 (2023).

[2] Y. Zhu, D. Peng, E. Zhang, B. Pan, X. Chen, L. Chen, H. Ren, F. Liu, Y. Hao, N. Li, Z. Xing, F. Lan, J. Han, J. Wang, D. Jia, H. Wo, Y. Gu, Y. Gu, L. Ji, W. Wang, H. Gou, Y. Shen, T. Ying, X. Chen, W. Yang, H. Cao, C. Zheng, Q. Zeng, J. Guo, and J. Zhao, Superconductivity in pressurized trilayer $\text{La}_4\text{Ni}_3\text{O}_{10-\delta}$ single crystals, *Nature* **631**, 531 (2024).

[3] M. Wang, H.-H. Wen, T. Wu, D.-X. Yao, and T. Xiang, Normal and superconducting properties of $\text{La}_3\text{Ni}_2\text{O}_7$, *Chin. Phys. Lett.* **41**, 077402 (2024).

[4] M. Zhang, C. Pei, D. Peng, X. Du, W. Hu, Y. Cao, Q. Wang, J. Wu, Y. Li, H. Liu, C. Wen, J. Song, Y. Zhao, C. Li, W. Cao, S. Zhu, Q. Zhang, N. Yu, P. Cheng, L. Zhang, Z. Li, J. Zhao, Y. Chen, C. Jin, H. Guo, C. Wu, F. Yang, Q. Zeng, S. Yan, L. Yang, and Y. Qi, Superconductivity in trilayer nickelate $\text{La}_4\text{Ni}_3\text{O}_{10}$ under pressure, *Phys. Rev. X* **15**, 021005 (2025).

[5] E. Zhang, D. Peng, Y. Zhu, L. Chen, B. Cui, X. Wang, W. Wang, Q. Zeng, and J. Zhao, Bulk superconductivity in pressurized trilayer nickelate $\text{Pr}_4\text{Ni}_3\text{O}_{10}$ single crystals, *Phys. Rev. X* **15**, 021008 (2025).

[6] M. Shi, D. Peng, K. Fan, Z. Xing, S. Yang, Y. Wang, H. Li, R. Wu, M. Du, B. Ge, Z. Zeng, Q. Zeng, J. Ying, T. Wu, and X. Chen, Pressure induced superconductivity in hybrid ruddlesden–popper $\text{La}_5\text{Ni}_3\text{O}_{11}$ single crystals, *Nature Physics* **21**, 1780 (2025).

[7] F. Li, Z. Xing, D. Peng, J. Dou, N. Guo, L. Ma, Y. Zhang, L. Wang, J. Luo, J. Yang, J. Zhang, T. Chang, Y.-S. Chen, W. Cai, J. Cheng, Y. Wang, Y. Liu, T. Luo, N. Hirao, T. Matsuoka, H. Kadobayashi, Z. Zeng, Q. Zheng, R. Zhou, Q. Zeng, X. Tao, and J. Zhang, Bulk superconductivity up to 96 k in pressurized nickelate single crystals, *Nature* **649**, 871 (2026).

[8] X. Chen, J. Choi, Z. Jiang, J. Mei, K. Jiang, J. Li, S. Agrestini, M. Garcia-Fernandez, H. Sun, X. Huang, D. Shen, M. Wang, J. Hu, Y. Lu, K.-J. Zhou, and D. Feng, Electronic and magnetic excitations in $\text{La}_3\text{Ni}_2\text{O}_7$, *Nat. Commun.* **15**, 9597 (2024).

[9] D. Zhao, Y. Zhou, M. Huo, Y. Wang, L. Nie, Y. Yang, J. Ying, M. Wang, T. Wu, and X. Chen, Pressure-enhanced spin-density-wave transition in double-layer nickelate $\text{La}_3\text{Ni}_2\text{O}_{7-\delta}$, *Sci. Bull.* **70**, 1239 (2025).

[10] Y. Li, Y. Cao, L. Liu, P. Peng, H. Lin, C. Pei, M. Zhang, H. Wu, X. Du, W. Zhao, K. Zhai, X. Zhang, J. Zhao, M. Lin, P. Tan, Y. Qi, G. Li, H. Guo, L. Yang, and L. Yang, Distinct ultrafast dynamics of bilayer and trilayer nickelate superconductors regarding the density-wave-like transitions, *Sci. Bull.* **70**, 180 (2025).

[11] J. Luo, J. Feng, G. Wang, N. N. Wang, J. Dou, A. F. Fang, J. Yang, J. G. Cheng, G.-q. Zheng, and R. Zhou, Microscopic evidence of charge- and spin-density waves in $\text{La}_3\text{Ni}_2\text{O}_{7-\delta}$ revealed by ^{139}La – NQR, *Chin. Phys. Lett.* (2025).

[12] R. Khasanov, T. J. Hicken, D. J. Gawryluk, V. Sazgari, I. Plokhikh, L. P. Sorel, M. Bartkowiak, S. Böttzel, F. Lechermann, I. M. Eremin, H. Luetkens, and Z. Guguchia, Pressure-enhanced splitting of density wave transitions in $\text{La}_3\text{Ni}_2\text{O}_{7-\delta}$, *Nat. Phys.* **21**, 430 (2025).

[13] M. Kakoi, T. Oi, Y. Ohshita, M. Yashima, K. Kuroki, T. Kato, H. Takahashi, S. Ishiwata, Y. Adachi, N. Hatada, T. Uda, and H. Mukuda, Multiband metallic ground state in multilayered nickelates $\text{La}_3\text{Ni}_2\text{O}_7$ and $\text{La}_4\text{Ni}_3\text{O}_{10}$ probed by ^{139}La -NMR at ambient pressure, *J. Phys. Soc. Jpn.* **93**, 053702 (2024).

[14] Y. Li, X. Du, Y. Cao, C. Pei, M. Zhang, W. Zhao, K. Zhai, R. Xu, Z. Liu, Z. Li, J. Zhao, G. Li, Y. Qi, H. Guo, Y. Chen, and L. Yang, Electronic correlation and pseudogap-like behavior of high-temperature superconductor $\text{La}_3\text{Ni}_2\text{O}_7$, *Chin. Phys. Lett.* **41**, 087402 (2024).

[15] C. C. Au-Yeung, X. Chen, S. Smit, M. Bluschke, V. Zimmermann, M. Michiardi, P. Moen, J. Kraan, C. S. B. Pang, C. T. Suen, S. Zhdanovich, M. Zonno, S. Gorovikov, Y. Liu, G. Levy, I. S. Elfimov, M. Berciu, G. A. Sawatzky, J. F. Mitchell, and A. Damascelli, Universal electronic structure of layered nickelates via oxygen-centered planar orbitals, *arXiv.2502.20450* (2025).

[16] Z. Liu, H. Sun, M. Huo, X. Ma, Y. Ji, E. Yi, L. Li, H. Liu, J. Yu, Z. Zhang, Z. Chen, F. Liang, H. Dong, H. Guo, D. Zhong, B. Shen, S. Li, and M. Wang, Evidence for charge and spin density waves in single crystals of $\text{La}_3\text{Ni}_2\text{O}_7$ and $\text{La}_3\text{Ni}_2\text{O}_6$, *Sci. China Phys. Mech. Astron.* **66**, 217411 (2022).

[17] Z. Liu, M. Huo, J. Li, Q. Li, Y. Liu, Y. Dai, X. Zhou, J. Hao, Y. Lu, M. Wang, and H.-H. Wen, Electronic correlations and partial gap in the bilayer nickelate $\text{La}_3\text{Ni}_2\text{O}_7$, *Nat. Commun.* **15**, 7570 (2024).

[18] Y. Meng, Y. Yang, H. Sun, S. Zhang, J. Luo, L. Chen, X. Ma, M. Wang, F. Hong, X. Wang, and X. Yu, Density-wave-like gap evolution in $\text{La}_3\text{Ni}_2\text{O}_7$ under high pressure revealed by ultrafast optical spectroscopy, *Nat. Commun.* **15**, 10408 (2024).

[19] G. He, J. Shen, S. Xie, H. Zhang, M. Huo, J. Shu, D. Hu, X. Zhou, Y. Zhang, L. Qin, L. Qiao, H. Liu, C. Hu, X. Dong, D. Wang, J. Liu, W. Hu, J. Yuan, Y.-J. Yan, Z. Qi, K. Jin, Z. Du, M. Wang, and D. Feng, Anisotropic electronic correlations in the spin density wave state of $\text{La}_3\text{Ni}_2\text{O}_7$, *Research Square* [10.21203/rs.3.rs-6952484/v1](https://doi.org/10.21203/rs.3.rs-6952484/v1) (2025).

[20] J. Zhang, D. Phelan, A. S. Botana, Y.-S. Chen, H. Zheng, M. Krogstad, S. G. Wang, Y. Qiu, J. A. Rodriguez-Rivera, R. Osborn, S. Rosenkranz, M. R. Norman, and J. F. Mitchell, Intertwined density waves in a metallic nickelate, *Nat. Commun.* **11**, 6003 (2020).

[21] S. Xu, C.-Q. Chen, M. Huo, D. Hu, H. Wang, Q. Wu, R. Li, D. Wu, M. Wang, D.-X. Yao, T. Dong, and N. Wang, Origin of the density wave instability in trilayer nickelate $\text{La}_4\text{Ni}_3\text{O}_{10}$ revealed by optical and ultrafast spectroscopy, *Phys. Rev. B* **111**, 075140 (2025).

[22] H. Li, X. Zhou, T. Nummy, J. Zhang, V. Pardo, W. E. Pickett, J. F. Mitchell, and D. S. Dessau, Fermiology and electron dynamics of trilayer nickelate $\text{La}_4\text{Ni}_3\text{O}_{10}$, *Nat. Commun.* **8**, 704 (2017).

[23] X. Du, Y. D. Li, Y. T. Cao, C. Y. Pei, M. X. Zhang, W. X. Zhao, K. Y. Zhai, R. Z. Xu, Z. K. Liu, Z. W. Li, J. K. Zhao, G. Li, Y. L. Chen, Y. P. Qi, H. J. Guo, and L. X. Yang, Correlated electronic structure and density-wave gap in trilayer nickelate $\text{La}_4\text{Ni}_3\text{O}_{10}$, [arXiv:2405.19853](https://arxiv.org/abs/2405.19853) (2024).

[24] D.-H. Gim, C. H. Park, and K. H. Kim, Orbital-selective quasiparticle depletion across the density wave transition in trilayer nickelate $\text{La}_4\text{Ni}_3\text{O}_{10}$, *Phys. Rev. Lett.* **135**, 136505 (2025).

[25] A. Suthar, V. Sundaramurthy, M. Bejas, C. Le, P. Puphal, P. Sosa-Lizama, A. Schulz, J. Nuss, M. Isobe, P. A. van Aken, Y. E. Suyolcu, M. Minola, A. P. Schnyder, X. Wu, B. Keimer, G. Khaliullin, A. Greco, and M. Hepting, Multiorbital character of the density wave instability in $\text{La}_4\text{Ni}_3\text{O}_{10}$, [arXiv:2508.06440](https://arxiv.org/abs/2508.06440) (2025).

[26] M. Li, J. Gong, Y. Zhu, Z. Chen, J. Zhang, E. Zhang, Y. Li, R. Yin, S. Wang, J. Zhao, D.-L. Feng, Z. Du, and Y.-J. Yan, Direct visualization of an incommensurate unidirectional charge density wave in $\text{La}_4\text{Ni}_3\text{O}_{10}$, *Phys. Rev. B* **112**, 045132 (2025).

[27] Q.-G. Yang, K.-Y. Jiang, D. Wang, H.-Y. Lu, and Q.-H. Wang, Effective model and s_{\pm} -wave superconductivity in trilayer nickelate $\text{La}_4\text{Ni}_3\text{O}_{10}$, *Phys. Rev. B* **109**, L220506 (2024).

[28] M. Zhang, H. Sun, Y.-B. Liu, Q. Liu, W.-Q. Chen, and F. Yang, s^{\pm} -wave superconductivity in pressurized $\text{La}_4\text{Ni}_3\text{O}_{10}$, *Phys. Rev. B* **110**, L180501 (2024).

[29] M. Zhang, H. Sun, Y.-B. Liu, Q. Liu, W.-Q. Chen, and F. Yang, Spin-density wave and superconductivity in $\text{La}_4\text{Ni}_3\text{O}_{10}$ under ambient pressure, *Phys. Rev. B* **111**, 144502 (2025).

[30] S. Deswal, D. Kumar, D. Rout, S. Singh, and P. Kumar, Dynamics of electron-electron correlation and electron-phonon coupled phase progression in trilayer nickelate $\text{La}_4\text{Ni}_3\text{O}_{10}$, *Applied Physics Letters* **127**, 071903 (2025).

[31] T. P. Devereaux and R. Hackl, Inelastic light scattering from correlated electrons, *Rev. Mod. Phys.* **79**, 175 (2007).

[32] N. Lazarević and R. Hackl, Fluctuations and pairing in Fe-based superconductors: light scattering experiments, *J. Phys.: Condens. Matter* **32**, 413001 (2020).

[33] J. Yang, H. Sun, X. Hu, Y. Xie, T. Miao, H. Luo, H. Chen, B. Liang, W. Zhu, G. Qu, C.-Q. Chen, M. Huo, Y. Huang, S. Zhang, F. Zhang, F. Yang, Z. Wang, Q. Peng, H. Mao, G. Liu, Z. Xu, T. Qian, D.-X. Yao, M. Wang, L. Zhao, and X. J. Zhou, Orbital-dependent electron correlation in double-layer nickelate $\text{La}_3\text{Ni}_2\text{O}_7$, *Nat. Commun.* **15**, 4373 (2024).

[34] S. Abadi, K.-J. Xu, E. G. Lomeli, P. Puphal, M. Isobe, Y. Zhong, A. V. Fedorov, S.-K. Mo, M. Hashimoto, D.-H. Lu, B. Moritz, B. Keimer, T. P. Devereaux, M. Hepting, and Z.-X. Shen, Electronic structure of the alternating monolayer-trilayer phase of $\text{La}_3\text{Ni}_2\text{O}_7$, *Phys. Rev. Lett.* **134**, 126001 (2025).

[35] Y. Li, Y. Cao, L. Liu, P. Peng, H. Lin, C. Pei, M. Zhang, H. Wu, X. Du, W. Zhao, K. Zhai, X. Zhang, J. Zhao, M. Lin, P. Tan, Y. Qi, G. Li, H. Guo, L. Yang, and L. Yang, Distinct ultrafast dynamics of bilayer and trilayer nickelate superconductors regarding the density-wave-like transitions, *Sci. Bull.* **70**, 180 (2025).

[36] J. Zhang, H. Zheng, Y.-S. Chen, Y. Ren, M. Yonemura, A. Huq, and J. F. Mitchell, High oxygen pressure floating zone growth and crystal structure of the metallic nickelates $R_4\text{Ni}_3\text{O}_{10}$ ($R = \text{La, Pr}$), *Phys. Rev. Mater.* **4**, 083402 (2020).

[37] X. Jia, Y. Shen, H. LaBollita, X. Chen, J. Zhang, Y. Li, H. Zhao, M. G. Kanatzidis, M. Krogstad, H. Zheng, A. H. Said, A. Alatas, S. Rosenkranz, D. Phelan, M. P. M. Dean, M. R. Norman, J. F. Mitchell, A. S. Botana, and Y. Cao, Lattice-charge coupling in a trilayer nickelate with intertwined density wave order, *Phys. Rev. X* **16**, 011013 (2026).

[38] R. Samnakay, D. Wickramaratne, T. R. Pope, R. K. Lake, T. T. Salguero, and A. A. Balandin, Zone-folded phonons and the commensurate-incommensurate charge-density-wave transition in $1T - \text{TaSe}_2$ thin films, *Nano Lett.* **15**, 2965 (2015).

[39] O. R. Albertini, R. Zhao, R. L. McCann, S. Feng, M. Terrones, J. K. Freericks, J. A. Robinson, and A. Y. Liu, Zone-center phonons of bulk, few-layer, and monolayer $1T - \text{TaS}_2$: Detection of commensurate charge density wave phase through Raman scattering, *Phys. Rev. B* **93**, 214109 (2016).

[40] G. He, L. Peis, E. F. Cuddy, Z. Zhao, D. Li, Y. Zhang, R. Stumberger, B. Moritz, H. Yang, H. Gao, T. P. Devereaux, and R. Hackl, Anharmonic strong-coupling effects at the origin of the charge density wave in CsV_3Sb_5 , *Nat. Commun.* **15**, 1895 (2024).

[41] H.-M. Eiter, M. Lavagnini, R. Hackl, E. A. Nowadnick, A. F. Kemper, T. P. Devereaux, J.-H. Chu, J. G. Analytis, I. R. Fisher, and L. Degiorgi, Alternative route to charge density wave formation in multiband systems, *Proc. Natl. Acad. Sci.* **110**, 64 (2013).

[42] M. Li, J. Gong, Y. Zhu, Z. Chen, J. Zhang, E. Zhang, Y. Li, R. Yin, S. Wang, J. Zhao, D.-L. Feng, Z. Du, and Y.-J. Yan, Direct visualization of an incommensurate unidirectional charge density wave in $\text{La}_4\text{Ni}_3\text{O}_{10}$, *Phys. Rev. B* **112**, 045132 (2025).

[43] Y. Gu, C. Le, Z. Yang, X. Wu, and J. Hu, Effective model and pairing tendency in the bilayer ni-based superconductor $\text{La}_3\text{Ni}_2\text{O}_7$, *Phys. Rev. B* **111**, 174506 (2025).

[44] C. Le, J. Zhan, X. Wu, and J. Hu, Opposite-mirror-parity scattering as the origin of superconductivity in strained bilayer nickelates, [arXiv:2501.14665](https://arxiv.org/abs/2501.14665) (2025).

[45] J. Yang, J. Zhan, T. Miao, M. Huo, Q. Xu, Y. Li, Y. Xie, B. Liang, N. Cai, H. Chen, W. Zhu, M. Xu, S. Zhang, F. Zhang, F. Yang, Z. Wang, Q. Peng, H. Mao, X. Li, Z. Zhu, G. Liu, Z. Xu, J. Hu, X. Wu, M. Wang, L. Zhao, and X. J. Zhou, Electronic origin of density wave orders in a trilayer nickelate, [arXiv:2601.22608](https://arxiv.org/abs/2601.22608) (2026).